Nb-substitution suppresses the superconducting critical temperature of pressurized MoB₂

J. Lim, S. Sinha, A. C. Hire, S. J. S. Kim, P. M. Dee, R. S. Kumar, D. Popov, R. J. Hemley, R. G. Hennig, R. J. Hirschfeld, G. R. Stewart, and J. J. Hamlin Department of Physics, University of Florida, Gainesville, Florida 32611, USA Department of Materials Science and Engineering,

University of Florida, Gainesville, Florida 32611, USA Quantum Theory Project, University of Florida, Gainesville, Florida 32611, USA Department of Physics, University of Illinois Chicago, Chicago, Illinois 60607, USA HPCAT, X-ray Science Division, Argonne National Laboratory, Argonne, Illinois 60439, USA Departments of Physics, Chemistry, and Earth and Environmental Sciences, University of Illinois Chicago, Chicago, Illinois 60607, USA (Dated: October 30, 2023)

A recent work has demonstrated that MoB₂, transforming to the same structure as MgB₂ (P6/mmm), superconducts at temperatures above 30 K near 100 GPa [C. Pei et al. Natl. Sci. Rev., nwad034 (2023)], and Nb-substitution in MoB₂ stabilizes the P6/mmm structure down to ambient pressure [A. C. Hire et al. Phys. Rev. B 106, 174515 (2022)]. The current work explores the high pressure superconducting behavior of Nb-substituted MoB₂ (Nb_{0.25}Mo_{0.75}B₂). High pressure x-ray diffraction measurements show that the sample remains in the ambient pressure P6/mmm structure to at least 160 GPa. Electrical resistivity measurements demonstrate that from an ambient pressure T_c of 8 K (confirmed by specific heat to be a bulk effect), the critical temperature is suppressed to 4 K at 50 GPa, before gradually rising to 5.5 K at 170 GPa. The critical temperature at high pressure is thus significantly lower than that found in MoB₂ under pressure (30 K), revealing that Nb-substitution results in a strong suppression of the superconducting critical temperature. Our calculations indeed find a reduced electron-phonon coupling in Nb_{0.25}Mo_{0.75}B₂, but do not account fully for the observed suppression, which may also arise from inhomogeneity and enhanced spin fluctuations.

I. INTRODUCTION

The discovery of superconductivity at a critical temperature $T_{\rm c}=39\,{\rm K}$ in MgB₂ [1] two decades ago sparked great interest in diborides amongst the scientific community. The superconductivity in this material is widely believed to be conventional in nature, *i.e.*, deriving from the electron-phonon interaction. The high critical temperature has been attributed at least partly to high phonon energy scales related to the presence of low mass (light) elements and to the significant covalent character of the states near the Fermi surface [2, 3].

A great deal of effort was focused on increasing the $T_{\rm c}$ to higher values by chemical substitution or pressure. These attempts were unsuccessful. Pressure causes a monotonic decrease in the $T_{\rm c}$ of MgB₂ [4, 5]. Similarly, partial substitutions on the Mg or B sites invariably cause a reduction of $T_{\rm c}$ [6, 7]. A number of structurally similar borides or borocarbides were also investigated, but none of these exhibited $T_{\rm c}$ values comparable to those found in MgB₂. A gradual decrease in further exploration of diboride superconductors followed. On the other hand, the search for high superconducting critical temperatures in light element compounds has been recommenced following the discovery of remarkably high $T_{\rm c}$ values in pressurized hydrides [8–10].

The recent discovery of superconductivity in MoB_2 with a T_c reaching as high as $32 \,\mathrm{K}$ at $110 \,\mathrm{GPa}$ has renewed the interest in diborides [11]. However, it has

been suggested that the mechanism of high $T_{\rm c}$ in MoB₂ is significantly different than that in MgB₂ [12]. At ambient pressure MoB₂ exists in an $R\overline{3}m$ structure, which is non-superconducting at low pressure. Above 25 GPa, however, superconductivity appears, with the highest $T_{\rm c}$ achieved in the P6/mmm phase (the same structure as MgB₂) at 110 GPa. These results led us to examine whether other diborides might also exhibit remarkably high critical temperatures at elevated pressures. In a recent paper [13], we reported that WB₂ reaches a maximum $T_{\rm c}$ of \sim 17 K at pressures near 90 GPa. Unlike MoB₂, bulk WB₂ adopts a $P6_3/mmc$ structure over the entire measured pressure range to at least 145 GPa. Our findings suggested that the superconducting nature of WB₂ derives from stacking faults in a MgB₂-like structure

An interesting question is whether the superconducting critical temperature of pressurized MoB_2 can be enhanced through chemical substitution. Our initial work in this direction has focused on examining the effects of partial Nb substitution on the Mo sites because NbB_2 occurs with P6/mmm structure in which MoB_2 superconducts above 30 K near 100 GPa. Recently, we showed, via density functional theory calculations, that phonon free energy stabilizes the P6/mmm structure relative to the $R\overline{3}m$ structure at high temperatures across the $\mathrm{Nb}_x\mathrm{Mo1}_{-x}\mathrm{B}_2$ series [14]. We were able to successfully synthesize Nb-substituted MoB_2 in the P6/mmm structure at ambient pressure via arc-

melting. The resulting compounds, $\mathrm{Nb}_{1-x}\mathrm{Mo}_x\mathrm{B}_2$, where x=0.1,0.25,0.5,0.75,0.9, were superconducting with $\mathrm{Nb}_{0.25}\mathrm{Mo}_{0.75}\mathrm{B}_2$ having the highest T_c of 8 K in the series. Specific heat measurements on the x=0.25 sample demonstrate bulk superconductivity and also showed a high upper critical field close to 7 T [14]. In the present study, we further investigate the superconductivity in Nb-substituted MoB_2 (x=0.25) through a combination of high-pressure electrical resistivity and x-ray diffraction measurements to pressures as high as 170 GPa.

II. METHODS

At lower pressures (< 2 GPa), we used a piston cylinder cell for resistivity measurements [15], with the Nb_{0.25}Mo_{0.75}B₂ sample ($\sim 1.0 \times 1.0 \times 0.4$ mm³) mounted in the van der Pauw configuration. A solution of n-pentane:isoamyl alcohol (1:1 ratio) was used as the pressure medium. Details on the use of the piston cylinder cell can be found in Ref. [16].

For higher pressure resistivity measurements, a micron-sized $Nb_{0.25}Mo_{0.75}B_2$ sample ($\sim 40 \times 40 \times 20 \,\mu\text{m}^3$) was placed in a gas membrane-driven diamond anvil cell (OmniDAC from Almax-EasyLab). A ruby crystal (20 µm in diameter) was used for pressure calibration [17] below 80 GPa. At higher pressures, the pressure was determined using the Raman spectrum of the diamond anvil [18]. Pressure was measured at 10 and 292 K during each cooling cycle within an error estimation of 5%. Two opposing diamond anvils (type Ia, 1/6carat, 0.15 mm central flats) and a cBN-epoxy, soapstone insulated Re metal gasket were used for the four-probe method (see inset in Fig. 1). The diamond anvil cell was then placed inside a customized continuous-flow cryostat (Oxford Instruments). For each temperature-dependent resistivity measurement, pressure was applied at room temperature. The sample was then cooled to 1.8 K before being warmed back to room temperature at a rate of $\sim 0.25 \,\mathrm{K/min}$. The measurements were performed with an excitation current of 0.3 mA. Further details of the non-hydrostatic high-pressure resistivity techniques are given in Refs. [13, 19].

High pressure x-ray diffraction measurements were performed on a powdered piece of $\mathrm{Nb}_{0.25}\mathrm{Mo}_{0.75}\mathrm{B}_2$ sample at beamline 16-BM-D at the Advanced Photon Source, Argonne National Laboratory. The x-ray beam had a wavelength of 0.41 Å (30 keV) in Runs 1 and 2, which was focused to a $3\times4\,\mu\mathrm{m}^2$ (FWHM) spot at the sample. A MAR345 image plate detector calibrated with a CeO_2 standard was used to record the diffracted intensity with the typical exposure time of 60 to 120 seconds per image. Neon was used as the pressure medium, and pressure was determined both using an online ruby fluorescence measurement [17] up to 40 GPa as well as the equation of state of Au grains [20] loaded into the sample chamber up to 162 GPa within an error estimation of 2%. DIOP-TAS [21] software was used to convert the 2D diffraction

images to 1D diffraction patterns which were further analyzed by Rietveld [22] and Le Bail [23] methods using GSAS-II software [24].

To better understand the superconducting properties of $\mathrm{Nb}_{0.25}\mathrm{Mo}_{0.75}\mathrm{B}_2$ under pressure we calculate the Allen-Dynes T_{c} at 100 GPa. The electron-phonon coupling constant, λ , was calculated from Eliashberg spectral function, $\alpha^2 F(\omega)$, obtained using the tetrahedron method as implemented in the density functional theory (DFT) code Quantum Espresso [25–27]. We use the Perdew–Burke-Ernzerhof functional for the exchange-correlation energy in the DFT calculations [28]. The virtual crystal approximation was used with the optimized norm-conserving pseudopotentials [29, 30]. A k-point mesh of $20 \times 20 \times 20$ and a q-point mesh of $4 \times 4 \times 4$ was used in the calculations.

III. RESULTS

The pressure-dependent resistivity curves of $\mathrm{Nb}_{0.25}\mathrm{Mo}_{0.75}\mathrm{B}_2$ are shown in Fig. 1 at 10, 150, and 292 K. While increasing pressure at 292 K, the resistivity was measured simultaneously at that temperature. However, the resistivity curves at 10 and 150 K were extracted from the temperature-dependent resistivity at different pressures (see inset in Fig. 2). There is no significant change in resistivity with respect to pressure indicating the absence of any structural phase transition. We also plot the resistivity in a base 10 logarithmic scale showing

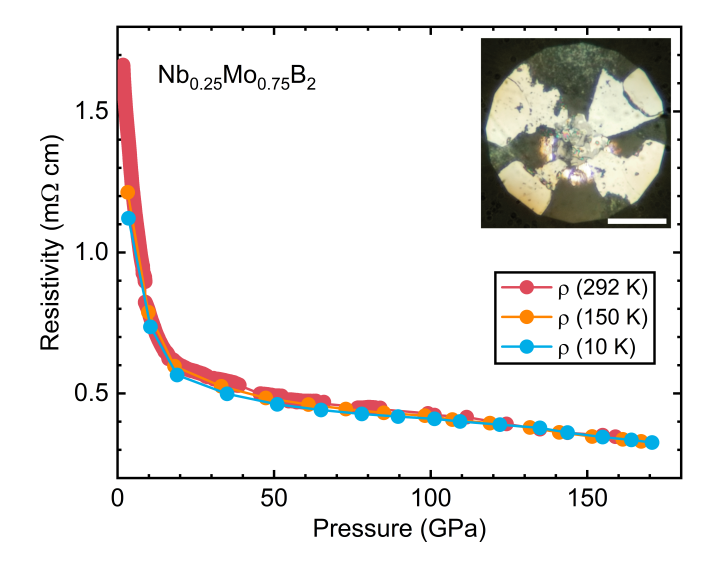


FIG. 1. Resistivity of $\mathrm{Nb_{0.25}Mo_{0.75}B_2}$ versus pressure to 171 GPa at 10, 150, and 292 K. The resistivity curves show no noticeable change with pressure indicating the absence of any structural phase transition. Pressures at 150 K were estimated, reflecting the small changes between pressures measured at 10 and 292 K. Inset shows the microphotograph of the sample, a ruby pressure calibrant, and the four-probe method looking through the upper diamond central flat (or culet). The white scale bar indicates 50 µm.

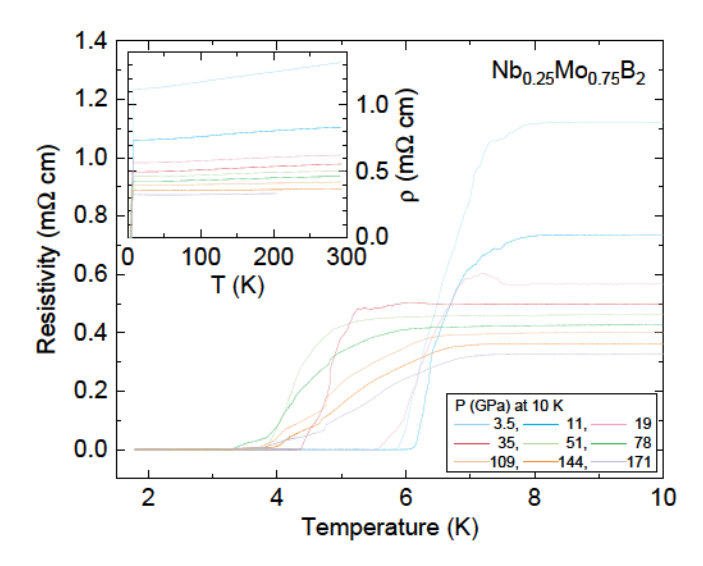


FIG. 2. Representative temperature-dependent resistivity curves of $\mathrm{Nb_{0.25}Mo_{0.75}B_2}$ under pressure to 171 GPa (measured at 10 K) clearly showing the zero resistivity of superconducting transition between 1.8-10 K during each warming cycle. Inset shows the full 1.8-292 K temperature range studied.

that the resistivity smoothly decreases with pressure (see Fig. S1 in the Supplemental Material [31]). The inset in Fig. 1 illustrates the four-probe electrical resistivity configuration in the diamond anvil cell looking through the upper diamond used in these measurements.

Figure 2 shows selected temperature-dependent resistivity curves under pressures up to 171 GPa (measured at 10 K) focusing on the superconducting transition. Nb_{0.25}Mo_{0.75}B₂ superconducts at ambient pressure with a $T_{\rm c}$ of 8 K as reported by our recent study [14]. Zero resistivity below the superconducting transition is observed in Nb_{0.25}Mo_{0.75}B₂ throughout the whole pressure range studied. The superconducting transition broadens significantly above 50 GPa. We denote the transition width ($\Delta T_{\rm c}$) by vertical bars in Fig. 3. The resistivity curve at 171 GPa in the inset of Fig. 2 ends at 200 K, where the diamonds failed during the warming cycle. Nevertheless, we managed to measure the highest pressure at 171 GPa using diamond anvil Raman at 10 K during the cooling cycle (see Fig. S2 in the Supplemental Material [31]).

The superconducting transition temperature (T_c) of Nb_{0.25}Mo_{0.75}B₂ versus pressure to 171 GPa from Run 1 (below 2 GPa including ambient pressure using a piston-cylinder cell) and Run 2 (above 2 GPa using a diamond anvil cell) is shown in Fig. 3. The $T_c(50\%)$ is defined by the temperature corresponding to the 50% of normal state resistivity value just above the superconducting transition (\sim 10 K), whereas the upper and lower vertical bars refer to the 90% and 0%(offset) criteria, respectively. The pressure-dependent superconducting transition temperature $(T_c(P))$ initially decreases with pressure with a slope of -0.067(6) K/GPa and above 50 GPa monotonically increases with a slope of 0.0097(6) K/GPa. In-

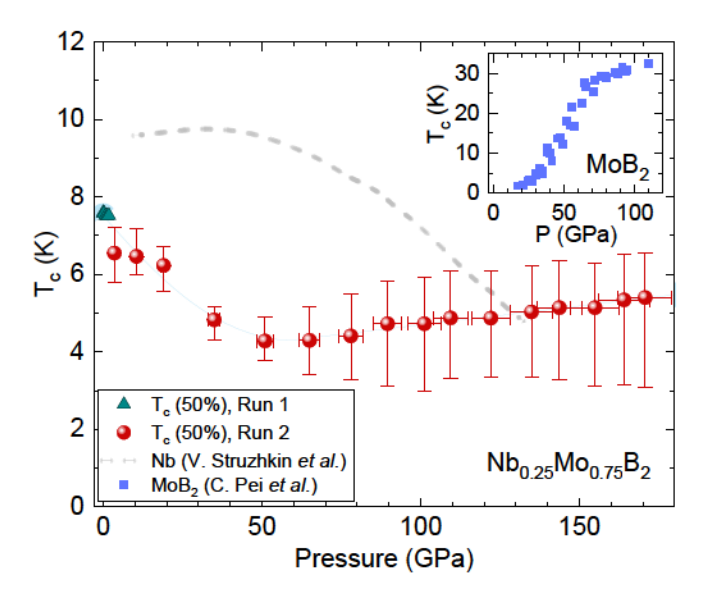


FIG. 3. Superconducting phase diagram of $\mathrm{Nb_{0.25}Mo_{0.75}B_2}$ to 171 GPa (measured at 10 K). The superconducting transition temperature ($T_{\rm c}$) initially goes down until ~ 50 GPa above which it monotonically increases up to 171 GPa. The upper and lower vertical bars refer to $T_{\rm c}(90\%)$ and $T_{\rm c}(\text{offset})$ respectively. The dashed line shows $T_{\rm c}(P)$ of elemental Nb for comparison [32]. Inset refers $T_{\rm c}(P)$ of pure MoB₂ from Ref. [11]

terestingly, the slope change in $T_{\rm c}({\rm P})$ above 50 GPa is accompanied by the significant broadening of superconducting transition width ($\Delta T_{\rm c}$), defined as the difference between $T_{\rm c}(90\%)$ and $T_{\rm c}({\rm offset})$ (see the corresponding vertical bars). The nonhydrostatic condition in the measurement partially contributes to the broadening due to the presence of the pressure gradient. However, the sudden increase above 50 GPa suggests the effect originates mainly from the sample itself. A comparison of $T_{\rm c}({\rm P})$ between Nb_{0.25}Mo_{0.75}B₂ and elemental Nb metal [32] is shown in Fig 3, which clearly demonstrates that the superconductivity in Nb_{0.25}Mo_{0.75}B₂ is not associated with Nb inclusions. Previous work has demonstrated that this material is a bulk superconductor [14].

In order to determine the presence of any structural transitions, we have performed synchrotron X-ray diffraction (XRD) measurements on powdered Nb_{0.25}Mo_{0.75}B₂ samples under high pressure and room temperature using Ne as a pressure transmitting medium in diamond anvil cells (DACs). Figure 4 shows a contour plot of XRD patterns whose intensities are normalized with the (101) peak in Runs 1 and 2. The P6/mmm structure at ambient pressure persists to pressures as high as 161 GPa as seen by the continued presence of the three dominant peaks with (001), (100), and (101) Miller indices. Vertically offset plots of the XRD patterns with respect to pressure from Runs 1 and 2 are shown in Fig. S3 in the supplemental material [31]. The peaks from the highly compressible Ne can be easily distinguished from those from the sample. The reflections from both Ne pressure medium and Re metal gasket are confirmed by their

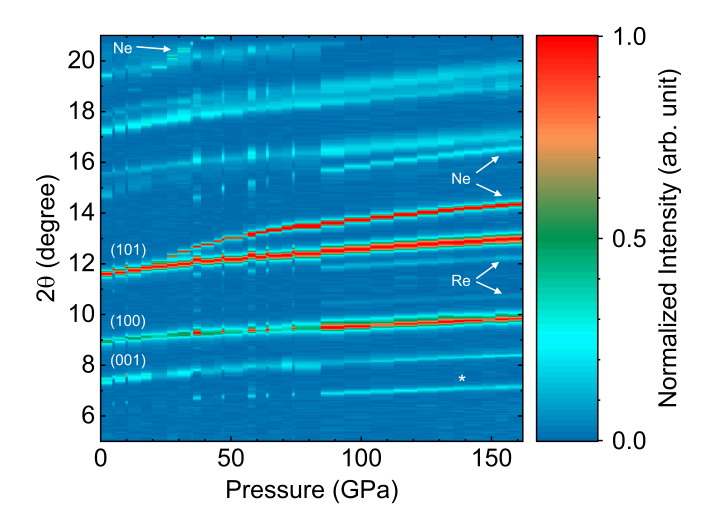


FIG. 4. Contour plot of XRD patterns of $Nb_{0.25}Mo_{0.75}B_2$ to 161 GPa at room temperature from Runs 1 and 2. The ambient structure (P6/mmm) persists up to the highest pressure without any structural phase transitions.

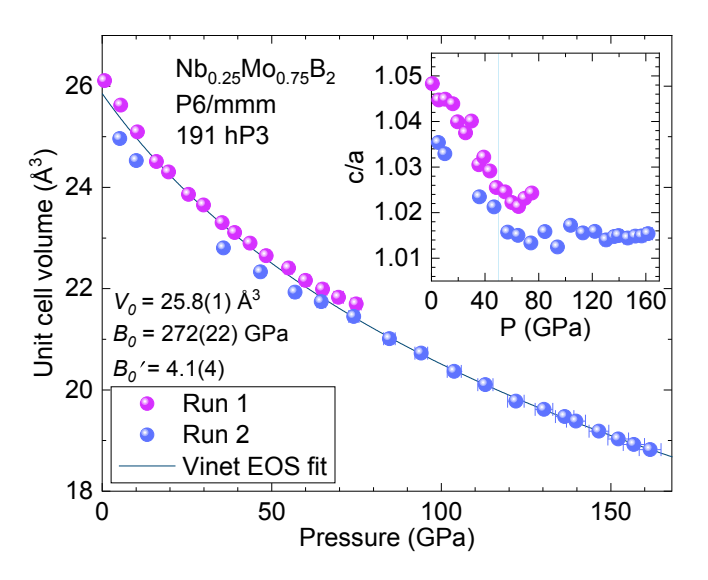


FIG. 5. P-V-isotherm of $\mathrm{Nb_{0.25}Mo_{0.75}B_2}$ to 161 GPa at room temperature. Inset shows the c/a ratio versus pressure. There is a slope change above ~ 50 GPa marked by a light blue shaded area referring to the potential correlation with the slope change of $T_c(\mathrm{P})$ in Fig. 3.

equation of state [33, 34]. There is a small amount of unidentified second phase between 6-7 degrees marked by a white asterisk (*).

The resulting pressure-volume (P-V) curve of $Nb_{0.25}Mo_{0.75}B_2$ in P6/mmm structure at room temperature from Runs 1 and 2 is shown in Fig. 5 with the c/a ratio versus pressure in the inset. There is a slope change in the c/a ratio above 50 GPa marked by a light blue shaded area, which seems to potentially correlate with the slope change in the $T_c(P)$ in Fig. 3. Interestingly, the value of the c/a ratio plateaus above 50 GPa, meaning that c lattice parameter begins to be

TABLE I. Calculated superconducting parameters. The critical temperatures, $T_{\rm c}$ were calculated using the Allen-Dynes equation with $\mu^*=0.16$. All the calculations utilized the P6/mmm structure. The DOS at the Fermi level is in units of states/eV/unit cell volume. (* indicates calculation was performed using the experimental lattice parameters.)

Material	Р	$N(E_{\rm F})$	ω_{log}	$\langle \omega^2 \rangle$	λ	$T_{\rm c}^{ m AD}$
	(GPa)		(K)	(K)		(K)
-NbB ₂	0	-	354	502.6	0.75	8.86
NbB_2	100	0.795	577.1	767.4	0.48	1.65
$Nb_{0.25}Mo_{0.75}B_2$	50	1.16	268.8	426.5	1.41	23.33
$Nb_{0.25}Mo_{0.75}B_2$	100	0.99	362.2	542.7	1.02	20.14
$Nb_{0.25}Mo_{0.75}B_2^*$	100	0.90	419.8	608.3	0.94	19.58
MoB_2	100	1.14	283.3	452.5	1.48	29.17

less compressible. This may indicate that the interaction between interlayers begins to play a significant role in the P6/mmm structure. The calculated a and c lattice parameters with respect to pressure are shown in Fig. S4 [31]. The Vinet Equation of state [35] is used to fit the P-V curve, which gives rise to an ambient volume 25.8 Å 3 (V_0), bulk modulus 272 GPa (B_0), and a derivative of the bulk modulus of 4.1 (B_0'). The bulk modulus of Nb_{0.25}Mo_{0.75}B₂ is comparable to that of MoB₂ (296 GPa) [36].

Table I shows the computed moments of phonon frequencies, the electron-phonon coupling parameter, and the Allen-Dynes $T_{\rm c}$ ($T_{\rm c}^{\rm AD}$) for NbB₂ (at 0 and 100 GPa), Nb_{0.25}Mo_{0.75}B₂ (at 50 and 100 GPa), and MoB₂ (at 100 GPa). According to these calculations, 25% Nb-substitution results in a moderate (roughly 30%) suppression of $T_{\rm c}$ compared to pure MoB₂ at 100 GPa. This occurs primarily due to a suppression of the electron-phonon coupling. Interestingly, the calculated $T_{\rm c}^{\rm AD}$ for Nb_{0.25}Mo_{0.75}B₂ at both 50 and 100 GPa appear to be overestimations when compared to the experimental $T_{\rm c}$. Contrary to the observed experimental trend, we found that $T_{\rm c}^{\rm AD}$ decreases as the pressure increases. Note that our x-ray diffraction results indicate that at 100 GPa, Nb_{0.25}Mo_{0.75}B₂ and MoB₂ adopt the same P6/mmm structure.

IV. DISCUSSION

One question that still follows from our experiment is why Nb-doped MoB₂ has a significantly lower transition temperatures than MoB₂ over the same pressure range studied in Ref. [11]. Much of the answer to this question can be gleaned from the literature on NbB₂, MoB₂, and alloyed transition metal diborides. We will focus on those findings which are most relevant for superconductivity, starting with the density of states (DOS) near the Fermi level. When compared with NbB₂, MoB₂ has a higher DOS near the Fermi level (Table I) and a higher fraction of electrons occupying antibonding states [37, 38]. This

difference helps to explain why, at ambient/low pressure, MoB_2 is a less stable diboride, preferring the trigonal $R\bar{3}m$ space group symmetry with alternating puckered boron planes instead of the hexagonal P6/mmm structure realized by NbB_2 [37]. In addition, MoB_2 has a higher isotropic electron-phonon coupling constant than NbB_2 [39–43]. Here, we would like to point out that the calculated electron-phonon coupling for NbB_2 at ambient pressure of $\lambda \sim 0.43$ in Singh [44] is a result of poorly converged calculations [41, 45], and our calculated value agrees with Heid et al. [41].

Another interesting aspect of the present study is that the experimentally realized suppression of $T_{\rm c}$ is at odds with the $T_{\rm c}^{\rm AD}$ obtained using the Allen-Dynes formula. The theory and experiment both qualitatively agree that Nb-substitution reduces the $T_{\rm c}$ in MoB₂ at high pressure (Table I) compared with MoB₂. However, there is significant quantitative disagreement in the magnitude of $T_{\rm c}$ between the two results. Experimentally, we found that Nb_{0.25}Mo_{0.75}B₂ at 100 GPa exhibits only about 30% of the $T_{\rm c}$ of pure MoB₂ at the same pressure (Table I). In contrast, the Allen-Dynes equation predicts that the Nb-substituted sample should exhibit about 70% of the $T_{\rm c}$ of pure MoB₂ (i.e., for Nb_{0.25}Mo_{0.75}B₂, $T_{\rm c}^{\rm AD}$ = 19.58 - 20.14 K; for MoB₂ $T_{\rm c}^{\rm AD}$ = 29.17 K). In other words, the Allen-Dynes $T_{\rm c}^{\rm AD}$ prediction works reasonably well for pure MoB₂, but it fails to capture the strong reduction in $T_{\rm c}$ for Nb-doped MoB₂.

Performing the same calculation for the T_c^{AD} of stoichiometric NbB2 at ambient pressure reveals a similar overestimation. However, in that case, the degree of overestimation is difficult to gauge since the experimental literature for stoichiometric NbB₂ is rife with inconsistencies. Some papers report $T_{\rm c}$'s between 0.62 K and 9 K [46–49], and many others report an absence of superconductivity down to the lowest temperatures measured [50-55]. There is considerably more evidence for finite T_c 's up to 8-11 K in nonstoichiometric NbB₂, characterized by increasing the ratio of B to Nb (enabled by Nb-vacancies) [49–52, 54–59] or decreasing this ratio via B-vacancies [60, 61]. Assuming that stoichiometric NbB₂ does not superconduct experimentally, except possibly at minimal temperatures, the Allen-Dynes prediction of $T_{\rm c}^{\rm AD} = 8.86 \text{ K}$ becomes a rather severe overestimation.

In light of the sensitivity to inhomogeneity and vacancy formation in NbB₂, we point out that MoB₂ is also susceptible to metal vacancy formation, which generally lowers the electronic density of states [43]. Taken together, we cannot rule out the role of inhomogeneities due to vacancies in the alloyed sample. Our calculations show that the tendency for metal vacancy formation in Nb_{0.25}M_{0.75}B₂ ($E_{\rm vf} = 0.214~{\rm eV}$) is even more likely than in NbB₂ ($E_{\rm vf} = 1.794~{\rm eV}$). The presence of vacancies on the 4d-atom site could lower the DOS at the Fermi level, reducing $T_{\rm c}$. While we do not include these effects in our calculations of the Eliashberg function, we suspect they play a role in the discrepancy between theory and experiment.

Another potential pathology leading to T_c predictions larger than experiment could stem from spin fluctuations absent from the present formalism. Several 3d transition metals like V and Cr are better known to have significant spin fluctuations [62–66]. While Nb is generally considered a conventional electron-phonon superconductor, some claim that spin fluctuations effects are essential for estimating T_c [64, 67]. We have used a modified McMillan formula defined in Eqn. (2) of Ref. [68] to estimate the electron-paramagnon coupling constant required to match the experimental T_c of $Nb_{0.25}Mo_{0.75}B_2$ (100 GPa), obtaining $\lambda_{\rm sf} \sim 0.15$. By comparison, to match a $T_c < 0.1 \text{ K}$ in NbB₂ (0 GPa) would require $\lambda_{\rm sf} > 0.26$. These values are comparable to results for Nb in Ref. [67] and provide at least a partial explanation for the $T_{\rm c}$ mismatch. Recent theoretical work on the itinerant antiferromagnet CrB₂ suggests that spin fluctuations are suppressed under pressure, giving rise to electron-phonon-mediated superconductivity at higher pressures [66]. It is unclear if Nb_{0.25}Mo_{0.75}B₂ exhibits analogous behavior in the pressure dependence of T_c in part due to the unknown role of other effects like disorder. Further theoretical investigations are necessary to pin down the sources of the overestimation of T_c , which is outside the scope of this study.

Our measured $T_{\rm c}$ values are comparable to those reported in many other stoichiometric and nonstoichiometric ternary diboride compounds (at ambient/low pressure), such as Mo_{0.95}Sc_{0.05}B₂ ($T_{\rm c}\approx 4.8$ K) [69], Mo_{0.96}Zr_{0.04}B₂ ($T_{\rm c}\approx 5.9$ K) [38], Zr_{0.96}V_{0.04}B₂ ($T_{\rm c}\approx 8.7$ K) [70], Zr_{0.96}Nb_{0.04}B₂ ($T_{\rm c}\approx 8.1$ K) [71], relevant doped binaries such as Nb_{1-x}B₂ ($T_{\rm c}\approx 9.2$ K) [51], NbB_x ($T_{\rm c}\approx 9.4$ K) [47], and many other borides of Mo and Nb in the range $T_{\rm c}\approx 0$ to 11.2 K [50]. There is considerably less literature studying diborides under pressures near 100 GPa, so it isn't easy to draw complete comparisons with the references above.

In nonstoichiometric NbB₂, increasing the B/Nb ratio tends to expand (shrink) the c(a) lattice parameter alongside a concomitant increase in T_c [43, 49–52, 54–59]. This behavior indicates that a smaller spacing along the c-axis is likely detrimental to superconductivity in NbB₂. Therefore, one can reasonably expect that the T_c of NbB₂ will decrease under pressure. Our T_c calculations further support this point, though the actual values are overestimates. In contrast, experiments by C. Pei et al. show that the T_c of MoB₂ rises sharply with applied pressure beyond 25 GPa until a structural transition near 70 GPa, where $T_{\rm c}$ continues to increase with pressure (and the c lattice parameter keeps decreasing) but at a lower rate [11]. Hence to achieve a higher T_c value, both the materials (NbB₂ and MoB₂) take advantage of different and opposing trends in the lattice parameters. This difference possibly explains the relatively flat T_c as a function of pressure observed in our experiments. Taken together, we can see that the role of Nb in $Nb_xMo_{1-x}B_2$ is to increase the low-pressure stability of the AlB₂ structure (P6/mmm) without recreating other conditions needed

for the higher $T_{\rm c}$ observed in MoB₂ under pressure.

V. CONCLUSIONS

In summary, we have studied the pressuredependent superconducting transition temperature of $Nb_{0.25}Mo_{0.75}B_2$ in the same structure as MgB_2 (P6/mmm). Electrical resistivity measurements up to 171 GPa reveal that $T_{\rm c}$ initially decreases with increasing pressure. Above 50 GPa, T_c increases monotonically with a significant broadening of transition width $\Delta T_{\rm c}$ up to the highest pressure. However, the ambient pressure T_c of 8 K is the highest T_c observed up to at least 171 GPa. Synchrotron high-pressure XRD measurements up to 161 GPa show that the slope of the c/a ratio changes above $50\,\mathrm{GPa}$ within the same P6/mmm structure, indicating a potential correlation with the change in slope of $T_{\rm c}({\rm P})$. Our theoretical findings show a reduction of $T_{\rm c}$, due to the weakened electron-phonon coupling, in $Nb_{0.25}Mo_{0.75}B_2$ compared to pure MoB_2 at high pressure, in qualitative agreement with the experiment. However, these calculations underestimate the observed suppression of T_c , suggesting that additional factors, such as inhomogeneity and spin fluctuations, may be present. High-pressure studies of other substitutions into MoB₂, which might enhance electron-phonon coupling, would be interesting to explore, to determine whether $T_{\rm c}$ values comparable to the 32 K observed in MoB₂ at 110 GPa [11] can be realized at low or ambient pressure.

Work at the University of Florida was performed under the auspices of U.S. Department of Energy Basic Energy Sciences under Contract No. DE-SC-0020385 and the U.S. National Science Foundation, Division of Materials Research under Contract No. NSF-DMR-2118718. A.C.H. and R.G.H. acknowledge additional support from the National Science Foundation under award PHY-1549132 (Center for Bright Beams). thank S. Tkachev (GSECARS, University of Chicago) for sample gas loading for the x-ray diffraction measurements, and C. Kenney-Benson (HPCAT) for technical assistance. R.S.K. and R.J.H. acknowledge support from the U.S. National Science Foundation (DMR-2119308 and DMR-2104881). X-ray diffraction measurements were performed at HPCAT (Sector 16), Advanced Photon Source (APS), Argonne National Laboratory. HP-CAT operations are supported by the DOE-National Nuclear Security Administration (NNSA) Office of Experimental Sciences. The beamtime was made possible by the Chicago/DOE Alliance Center (CDAC), which is supported by DOE-NNSA (DE-NA0003975). Use of the gas loading system was supported by COMPRES under NSF Cooperative Agreement No. EAR-1606856 and by GSE-CARS through NSF grant EAR-1634415 and DOE grant DE-FG02-94ER14466. The Advanced Photon Source is a DOE Office of Science User Facility operated for the DOE Office of Science by Argonne National Laboratory under Contract No. DE-AC02-06CH11357. High pressure equipment development at the University of Florida was supported by National Science Foundation CAREER award DMR-1453752.

ACKNOWLEDGMENTS

J. Nagamatsu, N. Nakagawa, T. Muranaka, Y. Zenitani, and J. Akimitsu, Nature 410, 63 (2001).

^[2] J. M. An and W. E. Pickett, Phys. Rev. Lett. 86, 4366 (2001).

^[3] I. Mazin and V. Antropov, Physica C: Superconductivity **385**, 49 (2003).

^[4] T. Tomita, J. J. Hamlin, J. S. Schilling, D. G. Hinks, and J. D. Jorgensen, Physical Review B 64, 092505 (2001).

^[5] S. Deemyad, T. Tomita, J. J. Hamlin, B. R. Beckett, J. S. Schilling, D. G. Hinks, J. D. Jorgensen, S. Lee, and S. Tajima, Physica C: Superconductivity 385, 105 (2003).

^[6] C. Buzea and T. Yamashita, Superconductor Science and Technology 14, R115 (2001).

^[7] S. L. Bud'ko and P. C. Canfield, Physica C: Superconductivity and its Applications 514, 142 (2015).

^[8] A. P. Drozdov, M. I. Eremets, I. A. Troyan, V. Ksenofontov, and S. I. Shylin, Nature 525, 73 (2015).

^[9] M. Somayazulu, M. Ahart, A. K. Mishra, Z. M. Geballe, M. Baldini, Y. Meng, V. V. Struzhkin, and R. J. Hemley, Phys. Rev. Lett. 122, 027001 (2019).

^[10] I. Osmond, O. Moulding, S. Cross, T. Muramatsu, A. Brooks, O. Lord, T. Fedotenko, J. Buhot, and

S. Friedemann, Phys. Rev. B 105, L220502 (2022).

^[11] C. Pei, J. Zhang, Q. Wang, Y. Zhao, L. Gao, C. Gong, S. Tian, R. Luo, M. Li, W. Yang, Z.-Y. Lu, H. Lei, K. Liu, and Y. Qi, Natl. Sci. Rev., nwad034 (2023) .

^[12] Y. Quan, K.-W. Lee, and W. E. Pickett, Phys. Rev. B 104, 224504 (2021).

^[13] J. Lim, A. C. Hire, Y. Quan, J. S. Kim, S. R. Xie, S. Sinha, R. S. Kumar, D. Popov, C. Park, R. J. Hemley, Y. K. Vohra, J. J. Hamlin, R. G. Hennig, P. J. Hirschfeld, and G. R. Stewart, Nat. Commun. 13, 7901 (2022).

^[14] A. C. Hire, S. Sinha, J. Lim, J. S. Kim, P. M. Dee, L. Fanfarillo, J. J. Hamlin, R. G. Hennig, P. J. Hirschfeld, and G. R. Stewart, Phys. Rev. B 106, 174515 (2022).

^[15] D. VanGennep, S. Maiti, D. Graf, S. W. Tozer, C. Martin, H. Berger, D. L. Maslov, and J. J. Hamlin, Journal of Physics: Condensed Matter 26, 342202 (2014).

^[16] I. R. Walker, Review of Scientific Instruments 70, 3402 (1999).

^[17] A. D. Chijioke, W. J. Nellis, A. Soldatov, and I. F. Silvera, Journal of Applied Physics 98, 114905 (2005).

^[18] Y. Akahama and H. Kawamura, Journal of Applied Physics 100, 043516 (2006).

^[19] T. Matsuoka and K. Shimizu, Nature 458, 186 (2009).

- [20] Y. Fei, A. Ricolleau, M. Frank, K. Mibe, G. Shen, and V. Prakapenka, Proceedings of the National Academy of Sciences 104, 9182 (2007).
- [21] C. Prescher and V. B. Prakapenka, High Pressure Research 35, 223 (2015).
- [22] H. M. Rietveld, Journal of Applied Crystallography 2, 65 (1969).
- [23] A. Le Bail, H. Duroy, and J. Fourquet, Materials Research Bulletin 23, 447 (1988).
- [24] B. H. Toby and R. B. Von Dreele, Journal of Applied Crystallography 46, 544 (2013).
- [25] P. Giannozzi, S. Baroni, N. Bonini, M. Calandra, R. Car, C. Cavazzoni, D. Ceresoli, G. L. Chiarotti, M. Cococcioni, I. Dabo, A. D. Corso, S. de Gironcoli, S. Fabris, G. Fratesi, R. Gebauer, U. Gerstmann, C. Gougoussis, A. Kokalj, M. Lazzeri, L. Martin-Samos, N. Marzari, F. Mauri, R. Mazzarello, S. Paolini, A. Pasquarello, L. Paulatto, C. Sbraccia, S. Scandolo, G. Sclauzero, A. P. Seitsonen, A. Smogunov, P. Umari, and R. M. Wentzcovitch, Journal of Physics: Condensed Matter 21, 395502 (2009).
- [26] P. Giannozzi, O. Baseggio, P. Bonfà, D. Brunato, R. Car, I. Carnimeo, C. Cavazzoni, S. de Gironcoli, P. Delugas, F. Ferrari Ruffino, A. Ferretti, N. Marzari, I. Timrov, A. Urru, and S. Baroni, The Journal of Chemical Physics 152, 154105 (2020).
- [27] P. Giannozzi, O. Andreussi, T. Brumme, O. Bunau, M. B. Nardelli, M. Calandra, R. Car, C. Cavazzoni, D. Ceresoli, M. Cococcioni, N. Colonna, I. Carnimeo, A. D. Corso, S. de Gironcoli, P. Delugas, R. A. DiStasio, A. Ferretti, A. Floris, G. Fratesi, G. Fugallo, R. Gebauer, U. Gerstmann, F. Giustino, T. Gorni, J. Jia, M. Kawamura, H.-Y. Ko, A. Kokalj, E. Küçükbenli, M. Lazzeri, M. Marsili, N. Marzari, F. Mauri, N. L. Nguyen, H.-V. Nguyen, A. O. de-la Roza, L. Paulatto, S. Poncé, D. Rocca, R. Sabatini, B. Santra, M. Schlipf, A. P. Seitsonen, A. Smogunov, I. Timrov, T. Thonhauser, P. Umari, N. Vast, X. Wu, and S. Baroni, Journal of Physics: Condensed Matter 29, 465901 (2017).
- [28] J. P. Perdew, K. Burke, and M. Ernzerhof, Phys. Rev. Lett. 77, 3865 (1996).
- [29] D. R. Hamann, Physical Review B 88, 10.1103/physrevb.88.085117 (2013).
- [30] M. Schlipf and F. Gygi, Computer Physics Communications 196, 36 (2015).
- [31] See Supplemental Material at [URL will be inserted by publisher] for extended figures and experimental details, such as electrical resistivity (log scale), pressure determination (Raman, sample P vs membrane P), x-ray diffraction patterns (stacked up), and calculated a and c lattice parameters (up to 162 GPa), respectively..
- [32] V. V. Struzhkin, Y. A. Timofeev, R. J. Hemley, and H.-k. Mao, Phys. Rev. Lett. 79, 4262 (1997).
- [33] A. Dewaele, F. Datchi, P. Loubeyre, and M. Mezouar, Phys. Rev. B 77, 094106 (2008).
- [34] S. Anzellini, A. Dewaele, F. Occelli, P. Loubeyre, and M. Mezouar, Journal of Applied Physics 115, 043511 (2014).
- [35] P. Vinet, J. Ferrante, J. H. Rose, and J. R. Smith, Journal of Geophysical Research: Solid Earth 92, 9319 (1987).
- [36] S. Yin, D. He, C. Xu, W. Wang, H. Wang, L. Li, L. Zhang, F. Liu, P. Liu, Z. Wang, C. Meng, and W. Zhu, High Pressure Research 33, 409 (2013).

- [37] P. Vajeeston, P. Ravindran, C. Ravi, and R. Asokamani1, Phys. Rev. B 63, 045115 (2001).
- [38] L. Muzzy, M. Avdeev, G. Lawes, M. Haas, H. Zandbergen, A. Ramirez, J. Jorgensen, and R. Cava, Physica C: Superconductivity 382, 153 (2002).
- [39] T. Oguchi, Journal of the Physical Society of Japan 71, 1495 (2002).
- [40] Y. G. Naidyuk, O. E. Kvitnitskaya, I. K. Yanson, S.-L. Drechsler, G. Behr, and S. Otani, Phys. Rev. B 66, 140301 (2002).
- [41] R. Heid, B. Renker, H. Schober, P. Adelmann, D. Ernst, and K.-P. Bohnen, Physical Review B 67 (2003).
- [42] I. R. Shein, N. I. Medvedeva, and A. L. Ivanovskii, Physics of the Solid State 45, 1617 (2003).
- [43] I. R. Shein and A. L. Ivanovskii, Phys. Rev. B 73, 144108 (2006).
- [44] P. P. Singh, Solid State Communications 125, 323 (2003).
- [45] P. P. Singh, Physical Review B 67 (2003).
- [46] L. Leyarovska and E. Leyarovski, Journal of the Less Common Metals 67, 249 (1979).
- [47] J. E. Schirber, D. L. Overmyer, B. Morosin, E. L. Venturini, R. Baughman, D. Emin, H. Klesnar, and T. Aselage, Phys. Rev. B 45, 10787 (1992).
- [48] H. Kotegawa, K. Ishida, Y. Kitaoka, T. Muranaka, N. Nakagawa, H. Takagiwa, and J. Akimitsu, Physica C: Superconductivity 378-381, 25 (2002).
- [49] H. Takeya, K. Togano, Y. S. Sung, T. Mochiku, and K. Hirata, Physica C: Superconductivity 408-410, 144 (2004).
- [50] A. S. Cooper, E. Corenzwit, L. D. Longinotti, B. T. Matthias, and W. H. Zachariasen, Proceedings of the National Academy of Sciences 67, 313 (1970).
- [51] A. Yamamoto, C. Takao, T. Masui, M. Izumi, and S. Tajima, Physica C: Superconductivity 383, 197 (2002).
- [52] R. Escamilla and L. Huerta, Superconductor Science and Technology 19, 623 (2006).
- [53] H. X. Geng, G. C. Che, W. W. Huang, S. L. Jia, H. Chen, and Z. X. Zhao, Superconductor Science and Technology 20, 452 (2007).
- [54] E. Regalado and R. Escamilla, Journal of Physics: Condensed Matter 19, 376209 (2007).
- [55] M. Mudgel, V. Awana, G. Bhalla, and H. Kishan, Solid State Communications 147, 439 (2008).
- [56] V. A. Gasparov, N. S. Sidorov, I. I. Zver'kova, and M. P. Kulakov, Journal of Experimental and Theoretical Physics Letters 73, 532 (2001).
- [57] R. Escamilla, O. Lovera, T. Akachi, A. Durán, R. Falconi, F. Morales, and R. Escudero, Journal of Physics: Condensed Matter 16, 5979 (2004).
- [58] C. A. Nunes, D. Kaczorowski, P. Rogl, M. R. Baldissera, P. A. Suzuki, G. C. Coelho, A. Grytsiv, G. André, F. Boureé, and S. Okada, Acta Materialia 53, 3679 (2005).
- [59] T. Takahashi, S. Kawamata, S. Noguchi, and T. Ishida, Physica C: Superconductivity 426-431, 478 (2005).
- [60] J. K. Hulm and B. T. Matthias, Phys. Rev. 82, 273 (1951).
- [61] W. T. Ziegler and R. A. Young, Phys. Rev. 90, 115 (1953).
- [62] J. Castaing, P. Costa, M. Heritier, and P. Lederer, Journal of Physics and Chemistry of Solids 33, 533 (1972).
- [63] A. Bauer, A. Regnat, C. G. F. Blum, S. Gottlieb-Schönmeyer, B. Pedersen, M. Meven, S. Wurmehl,

- J. Kuneš, and C. Pfleiderer, Phys. Rev. B 90, 064414 (2014).
- [64] K. Tsutsumi, Y. Hizume, M. Kawamura, R. Akashi, and S. Tsuneyuki, Phys. Rev. B 102, 214515 (2020).
- [65] C. Pei, P. Yang, C. Gong, Q. Wang, Y. Zhao, L. Gao, K. Chen, Q. Yin, S. Tian, C. Li, W. Cao, H. Lei, J. Cheng, and Y. Qi, arxiv:2109.15213 [cond-mat.suprcon] (2021).
- [66] S. Biswas, A. Kreisel, A. Valadkhani, M. Dürrnagel, T. Schwemmer, R. Thomale, R. Valentí, and I. I. Mazin, arxiv:2211.01054 [cond-mat.supr-con] (2022).
- [67] S. K. Bose, Journal of Physics: Condensed Matter 21, 025602 (2008).
- [68] I. I. Mazin, D. A. Papaconstantopoulos, and M. J. Mehl, Phys. Rev. B 65, 100511 (2002).

- [69] W. Yang, G. Xiao, Q. Zhu, Y. Cui, S. Song, G.-H. Cao, and Z. Ren, Ceramics International 48, 19971 (2022).
- [70] S. T. Renosto, H. Consoline, C. A. M. dos Santos, J. Albino Aguiar, S.-G. Jung, J. Vanacken, V. V. Moshchalkov, Z. Fisk, and A. J. S. Machado, Phys. Rev. B 87, 174502 (2013).
- [71] M. D. R. Marques, F. S. Portela, L. T. Corredor, G. Zhang, J. Vanacken, V. V. Moshchalkov, L. E. Correa, S. T. Renosto, O. Cigarroa, A. J. S. Machado, and J. A. Aguiar, Superconductor Science and Technology 29, 095007 (2016).